International Journal of Fluid Power 6 (2005) No. 3 pp. 33-43

# MODELLING OF A NOZZLE-FLAPPER TYPE PNEUMATIC SERVO VALVE INCLUDING THE INFLUENCE OF FLOW FORCE

**Tao Wang, Maolin Cai, Kenji Kawashima and Toshiharu Kagawa**

*Department of Mechano-Micro Engineering, Tokyo Institute of Technology, Nagatsuta-cho 4259, Midori-ku, Yokohama 226-8503, Japan*
*wangtao@k-k.pi.titech.ac.jp, caiml@k-k.pi.titech.ac.jp, kkawashi@pi.titech.ac.jp, kagawa@pi.titech.ac.jp*

**Abstract**

This paper proposed a nonlinear mathematical model for a 4-port pneumatic nozzle-flapper type servo valve with dual fixed orifices and dual nozzles. In this model, the influence of the flow force was also included. The determination of the flow force on the flapper was proposed using an experimental approach. The effectiveness of the proposed model was verified by comparing experimental and simulated results. This comparison confirmed the influence of flow force on the static and dynamic behavior of the servo valve. A linear model, which was derived from the nonlinear model, showed an applicable range of about ±30 % of rated input current. A practical, order-reduced linear model, which neglects the dynamics of the torque motor and the armature-flapper, was also proposed. The order-reduced model was suitable for systems with large load volumes.

**Keywords:** nozzle-flapper type pneumatic servo valve, nonlinear model, flow force, linear model

## 1 Introduction

In pneumatic position and force control systems, nozzle-flapper type servo valves are normally used for obtaining quick response and precise control results due to their simple structure, high sensitivity and wide frequency range (Shearer, 1956). Pneumatic control systems with nozzle-flapper elements are generally approximated to a first order lag system assuming an isothermal state change for the air in the load chamber (Zalmanzon, 1965; Kagawa, 1985). Nozzle-flapper type servo valves are usually treated as a proportional element when neglecting torque motor dynamics and flow force on the flapper (Thayer, 1958). At present, there is no general mathematical model to describe a 4-port nozzle-flapper type electronic-pneumatic servo valve with dual fixed orifices and dual nozzles, though the pneumatic servo valve is almost equivalent to the first stage of common electro-hydraulic servo valves (Lin and Akers, 1991; Urata et al, 1998; Kim and Tsao, 2000; Grodić et al, 2004).

Recently, the demand on electric power saving for servo valve has been increasing as part of energy saving campaign. However, this leads to the inadequate driving power of the torque motor. Consequently, the influence of flow force on the properties of these valves has become more and more significant. For nozzle-flapper type hydraulic servo valves, methods for calculating the flow force have been established (Merritt, 1967; Urata and Yamashina, 1998). However, the flow force on the flapper, generated by the air-jet from the nozzle, cannot be readily calculated from physical geometry due to the compressibility of air. Numerical analyses of the pressure distribution on the flapper have been conducted for a few specific nozzle and flapper geometries and supply pressures (Araki, 1965; Crnojevic, 1997). However, it is very difficult to give a general expression of the flow force for different nozzle geometries, though an approximate equation for calculating the flow force has been proposed using an experimental approach (Zhang et al, 2003).

In some high precision pressure control systems, e.g. exposure apparatuses which are actively isolated using air-springs (Wakui, 2003), an accurate model of the servo valve is required for the design of the system dynamics.

In this paper, general nonlinear and linear models are proposed which include the influence of flow force.

First, a nonlinear dynamic model for a 4-port nozzle-flapper type pneumatic servo valve is derived. This includes the influence of flow force on the flapper. In addition, a practical determination method for flow

This manuscript was received on 9 May 2005 and was accepted after revision for publication on 15 September 2005

force is proposed using an experimental approach. Then the complete nonlinear model and a simplified model neglecting flow force are simulated and the simulation results of both models are compared with the experimental results for consistent conditions. By linearizing the nonlinear model around its equilibrium state, a linear model is then derived. A practical, order-reduced, linear model is also proposed which neglects the dynamics of the torque-motor and armature-flapper. Simulation results of various step responses are then compared with those of experiments.

## 2 Operation of Nozzle-flapper Type Pneumatic Servo Valves

The basic construction of a 4-port nozzle-flapper type servo valve is shown in Fig. 1. The armature-flapper is moved by a torque motor consisting of a coil and vertically arranged magnets. Movement of the flapper changes the distance between it and both nozzles. This creates different pressures, $P_{c1}$ and $P_{c2}$, in the control sides. In the steady state, the differential pressure, $\Delta P=P_{c1}-P_{c2}$, is proportional to the input current when the control ports are closed.

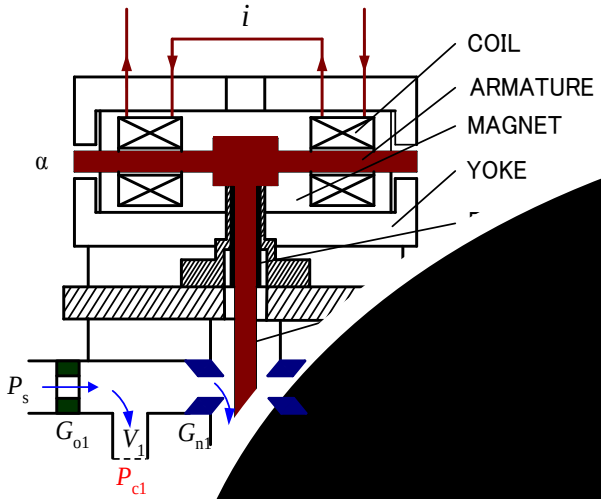


**Fig. 1:** *The basic construction of a 4-port nozzle-flapper type pneumatic servo valve*

The servo valve used in our experiment is part AS121005 as manufactured by PSC Company. The range of control pressure change is 300~400 kPa for the rated current of ±100 mA and air supply pressure of 400 kPa. The rated differential pressure is –8.6 kPa for an input current of 10 mA.

## 3 Dynamic Model of a Pneumatic Servo Valve

### 3.1 Torque Motor and Armature-Flapper

First, the dynamic model for the electric-drive section of the servo valve is investigated. The one-degree of freedom model of the armature-flapper is shown in Fig. 2 (Urata, 1999). The current in the coil generates a torque driving the armature-flapper. The relationship between the input current and the torque, including the influence of eddy currents, is given by (Urata, 2004):

$$T_e\dot{T}_t + T_t = K_m\alpha + K_i i \tag{1}$$

The torque on the armature-flapper, caused by the flex-tube which acts as an elastic support, is proportional to the rotation of the armature-flapper, described as follows:

$$T_s = K_a\alpha \tag{2}$$

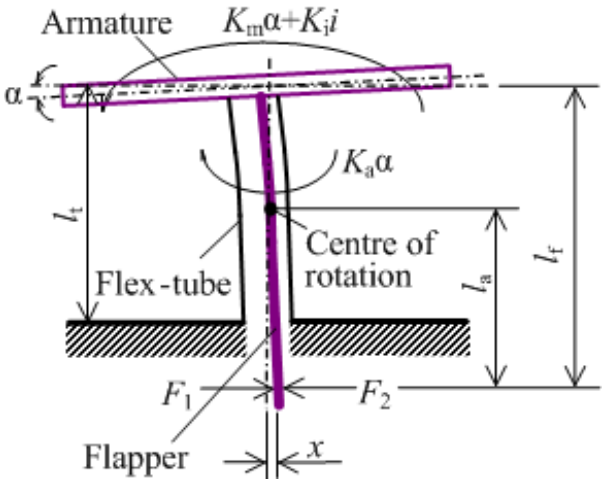


**Fig. 2:** *One-degree of freedom model of the armature-flapper*

The torque on the flapper around the centre of rotation, caused by flow forces which are generated by air jet from the two nozzles, is given by (Urata, 2004):

$$T_f = (F_1 - F_2)l_a \tag{3}$$

where

$$l_a = l_f - l_t/2$$

Summing moments about the centre of rotation, we obtain:

$$J\ddot{\alpha} = T_t - T_s + T_f - B_t\dot{\alpha} \tag{4}$$

The flapper tip displacement depends upon the inclinations and deflections of the flex-tube and the flapper (Urata and Yamashina, 1998; Urata, 2004):

$$x = \alpha l_a + (F_1 - F_2)(1/K_F + 1/K_T) \tag{5}$$

### 3.2 Flow Rate Characteristics

The flow through the fixed orifice and the nozzle-flapper can be sonic or subsonic depending upon the upstream/downstream pressure ratio. The mass flow rate through a restriction is a function of geometric parameters, the upstream and downstream pressures. To express the mass flow rate, we adopt the following expression in this paper (Oneyama et al, 2003):

$$G = C\rho P_u\varphi(P_u, P_d) \tag{6}$$

where

$$\varphi(P_u, P_d) = \begin{cases} 1 & P_d/P_u \le b \\ \left\{1 - \left(\dfrac{P_d/P_u - b}{1-b}\right)^2\right\}^m & P_d/P_u > b \end{cases} \quad (7)$$

For this expression, $C$, $b$ and $m$ are named sonic conductance, critical pressure ratio and subsonic index respectively. Three coefficients, $C_o$, $b_o$, $m_o$, are constants for the fixed orifices. The critical pressure ratio, $b_n$, and the subsonic index, $m_n$, change slightly with surrounding geometric dimensions of the nozzle-flappers. However, the influence of these changes on the flow rate characteristic is small. Therefore, we assume a constant critical pressure ratio and a constant subsonic index for the nozzle-flapper. The sonic conductance, $C_n$, is approximately proportional to the gap between the nozzle and the flapper and is expressed by

$$C_n = \begin{cases} C_{n0}(x_f + x)/x_f; & \text{for right nozzle - flapper} \\ C_{n0}(x_f - x)/x_f; & \text{for left nozzle - flapper} \end{cases} \quad (8)$$

where $C_{n0}$ is the sonic conductance of the nozzle-flapper at zero input current.

### 3.3 Flow Force on the Flapper

The flow model at the nozzle-flapper of the specific servo valve is shown in Fig. 3 in the case of $P_c \ge P_a/b_n$ . The air velocity reaches a maximum value up to the local speed of sound at the exit section 2 (Araki, 1965; Crnojevic, 1997).

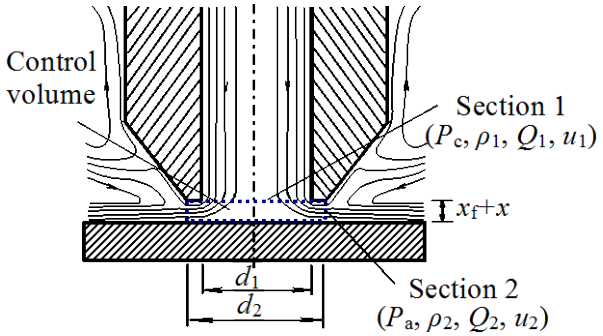


**Fig. 3:** *Flow model at nozzle-flapper*

Applying momentum theory to control surface shown in Fig. 3, we can obtain the flow force, $F_f$, acting on the flapper when neglecting the velocity of the flapper tip (Ohuchi and Ikebe, 1980; Urata, 1998).

$$F_f = P_c A_1 + \rho_1 Q_1 u_1 - (P_a A_2 + \rho_2 Q_2 u_2) \quad (9)$$

where, $P_c$ and $P_a$, $\rho_1$ and $\rho_2$, $Q_1$ and $Q_2$, $u_1$ and $u_2$ are pressures, densities, volume flow rates and velocities at section 1 and 2 respectively. And $A_1 = \pi d_1^2/4$ , $A_2 = \pi d_2 (x_f + x)$.

Because $A_2 << A_1$ and $u_1 << u_2$, the second and third terms in Eq. 9 can be neglected. Substituting the local speed of sound at section 2, $u_2 = \sqrt{2(\kappa/(\kappa+1))P_c/\rho_1}$ , and air volume flow rate, $Q_2 = K_n u_2 A_2$ , into Eq. 9, we obtain

$$F_f = P_c A_1 - 2\rho_2 K_n A_2 (\kappa/(\kappa+1))P_c/\rho_1 \quad (10)$$

where $K_n$ is the air flow rate coefficient which depends upon the ratio of $A_2$ and $A_1$. Assume $K_n \propto (A_2/A_1)^2$ (Toyokura and Kamemoto, 1976). Thus, Eq.10 can be rewritten as:

$$F_f = \left(1 - f_1\left(\frac{x_f + x}{x_f}\right)^3\right) P_c A_1 \quad (11)$$

where the coefficient $f_1$ is estimated by the following method.

The flow force expression is verified and the coefficient is estimated in Eq. 11 using the experimental approach shown in Fig. 4:

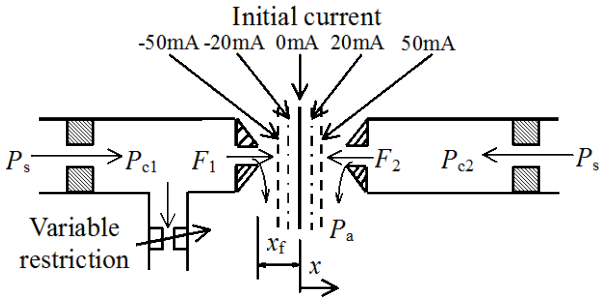


**Fig. 4:** *Experimental apparatus for measuring flow force*

Given a displacement of the flapper, we first investigate the relationship between the flow force and the control pressure. Because a direct measurement of the flow force on the flapper is not available, compensation current is used to represent the actual flow force.

To determine the flow force on the left side of flapper, the right control port is closed and a variable restriction is connected to the left control port, as shown in Fig. 4. Applying an initial current to the servo valve, an increase of the variable restriction passage area decreases the control pressure $P_{c1}$. Simultaneously, the flow force moving the flapper to the left causes a decrease of the control pressure at the right side. In order to hold the initial position of the flapper, compensation is applied to the input current to maintain the initial value of the control pressure at the right side. For this condition, we can also consider the flapper to be in its initial position.

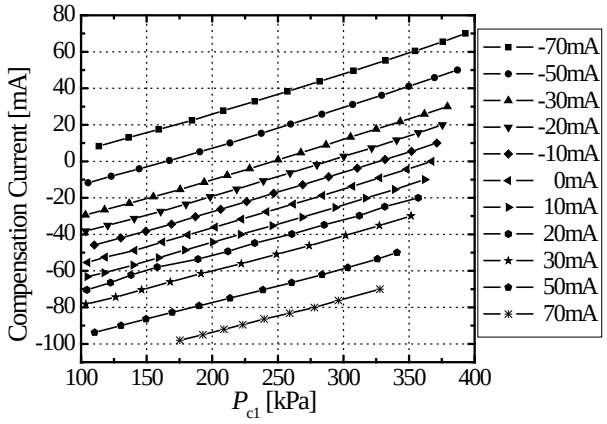

**Fig. 5:** *Compensation current vs. control pressure*

Figure 5 shows that the relationship between the compensation current and the control pressure is approximately linear, as the variable restriction passage area for initial input currents from –70 to 70 mA changes. Thus, when the distance between the flapper and the nozzle is held constant, the linear relationship between the flow force and the control pressure can be verified as Eq. 11 and can be written as follows:

$$F_1 = \left(1 - f_1\left(\frac{x_f + x}{x_f}\right)^3\right) P_{c1} A_1 = K_{f1} P_{c1} \tag{12}$$

By eliminating the dynamics of the torque motor and armature-flapper in Eq. 4, the coefficient, $K_{f1}$, can be obtained:

$$K_{f1} = \frac{K_i}{l_a} \frac{\Delta i}{\Delta P_{c1}} \tag{13}$$

$K_{f1}$ changes with the initial displacement of the flapper. Because a direct measurement of flapper displacement is difficult in an operating condition, we estimate it using the control pressure. When the both control ports are closed, the flow is sonic at the nozzle-flappers; the flow is subsonic at the fixed orifices. Since the flow rate through the fixed orifice is equal to that through the nozzle-flapper, we have the following equation with respect to the left side flow;

$$C_{o1} \rho P_s \varphi(P_s, P_{c1}) = C_{n10} \frac{x_f + x}{x_f} \rho P_{c1} \varphi(P_{c1}, P_a) \tag{14}$$

Thus, we can determinate the nodimensional displacement, $(x_f + x)/x_f$ , by substituting a measured value of $P_{c1}$ into the above equation. Figure 6 shows the change in the gradient of Fig. 5, $\Delta i/\Delta P_{c1}$ or $K_{f1} l_a / K_i$ , with nondimensional displacement.

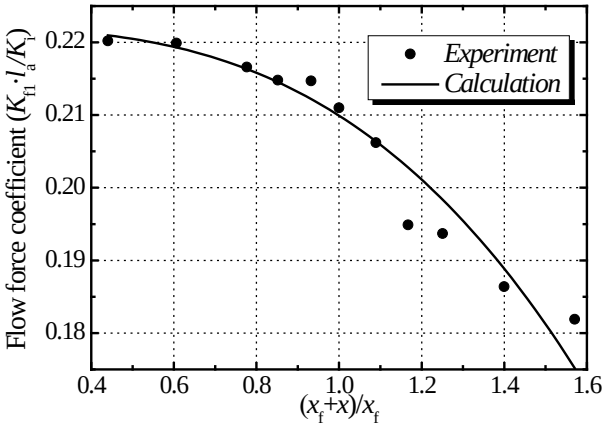


**Fig. 6:** *Flow force coefficient vs. nondimensional displacement*

The coefficient, $K_{f1}$, reduces as the distance between the flapper and the nozzle increases. Substituting the experimental results into Eq.12, we can estimate the coefficient, $f_1$, using the least square principle. There is a good agreement with the experiment and calculation results from Fig. 6. The flow force on the right side of the flapper can be similarly obtained:

$$F_2 = K_{f2} P_{c2} \tag{15}$$

where

$$K_{f2} = \left(1 - f_1\left(\frac{x_f - x}{x_f}\right)^3\right) A_1$$

### 3.4 Air Dynamics in the Control Chamber

The servo valve construction (Fig. 1) shows that, when the control ports are closed, there are small chambers ($V_1$ and $V_2$) between the fixed orifice and the nozzle. Assuming sufficient heat transfer between the air and the wall of the chamber, and recognizing the small volume of the chamber, the air temperature change inside the chamber is assumed to be isothermal. Thus, the flow rate change in the chamber is obtained from the air state equation:

$$G_c = \dot{P}_c / K_c \tag{16}$$

where

$$K_c = R\theta / V$$

Applying the continuity equation to the 4-port nozzle-flapper servo valve, the following equation can be obtained:

$$G_c = G_o - G_n \tag{17}$$

$G_c$, $K_c$, $V$, $P_c$, $G_o$ and $G_n$ for the left and right side of flapper are expressed by attaching the subscripts 1 and 2 respectively.

## 4 Simulation and Experiment

### 4.1 Simulation Structure

From the above analysis, we can establish a simulation model from Eq. 4-8, 16 and 17, as shown in Fig. 7. The input is the current, $i$, while the outputs are the control pressures, $P_{c1}$ and $P_{c2}$ (or differential pressure $\Delta P$). The flow states at the fixed orifice and the nozzle-flapper are determined to be subsonic or sonic by comparing the actual pressure ratio to the critical pressure ratio. Changing the control pressure from atmospheric to the supply pressure results in three possible flow state combinations, as illustrated in Table 1.

**Table 1:** Air flow state at the orifice and nozzle-flapper

| | I | II | III |
|---|---|---|---|
| at fixed orifice | sonic | sonic | subsonic |
| at nozzle-flapper | subsonic | sonic | sonic |

Among all of the parameters of the models, the armature-flapper dynamic coefficients, $T_e$, $B_f$, $K_F$ and $K_T$ were selected for comparison with the experimental results. The coefficients in the flow force calculation equations were estimated using the experimental ap-

proach described in section 3.3. The coefficients in the flow rate equation of the fixed orifice and the nozzle-flapper, $C_o$, $b_o$, $m_o$ and $C_{n0}$, $b_n$, $m_n$, were determined through the improved flow rate measurement method of pneumatic components (Oneyama, 2003). The other parameters were determined from the physical properties of the valve.

### 4.2 Results

To validate the derived model, a Matlab/Simulink model of the system shown in Fig. 7 was constructed and simulated. The results thereof were compared with experimental results under the same conditions. The experiments were performed at a constant ambient temperature of 20 °C and a supply pressure of 400 kPa. Additionally, in order to clarify the influence of flow force, a model which excluded the flow force was simulated. The simulation results were compared to those of the previous simulation and experiment.

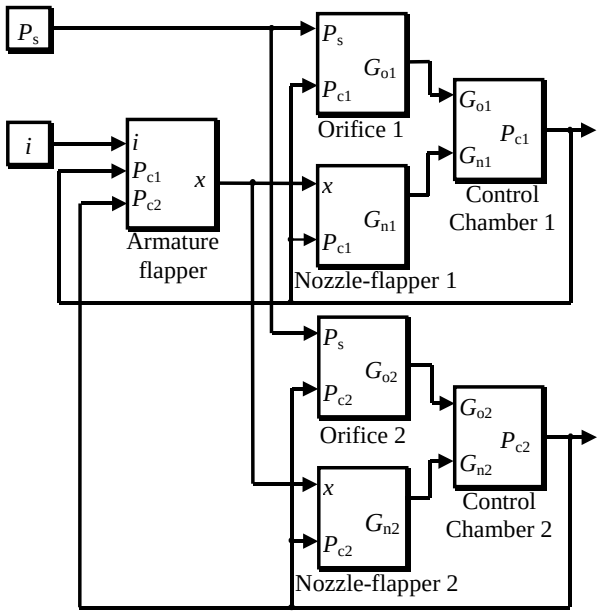


**Fig. 7:** *Simulation model for a 4-port nozzle-flapper type pneumatic servo valve*

The steady-state control pressures, $P_{c1}$ and $P_{c2}$, and their differential pressure, $\Delta P$, were plotted against input current, $i$ (no load flow rate), as shown in Fig. 8. With both of the control ports closed, the input current was varied using a triangular waveform varying between ±100mA at 1/120Hz.

Figure 8 shows good agreement between simulation and experiment, despite some hysteresis and a slight deviation at both ends of the experimental curve. This is thought to be due to the negligence of the torque motor hysteresis in the simulation and also flow rate calculation errors at maximum and minimum input currents. There is an almost linear relationship between the input current and differential pressure.

For the results neglecting the flow force, the change of differential pressure with respect to input current was in excess of the experimental results. This can be explained by noting from Eq. 4 and 5 that neglecting the flow force on the flapper naturally leads to larger displacements of the flapper than for the real system. In spite of this, the error remains within 35% of the actual results.

Another steady-state response is obtained by plotting flow rate at the control port versus the control pressure. For various input currents (-30, 0 and 30 mA), the load pressure at one of the side ports was slowly varied from atmospheric to the supply pressure while the other port remained closed. Flow rate changes with increasing the load pressure are shown in Fig. 9 for the case of load pressure changes to the left control port with the right port closed. Positive and negative values for the flow rate indicate flows out of and into the servo valve respectively.

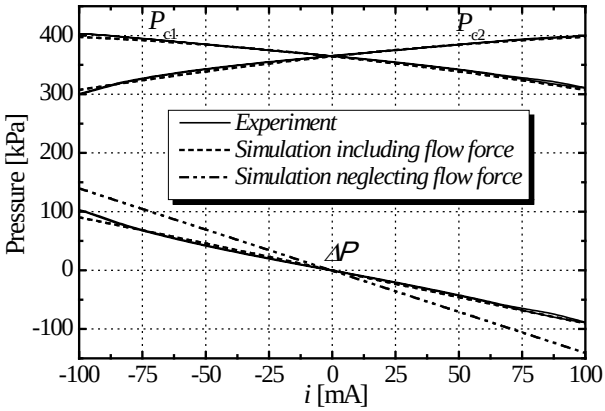


**Fig. 8:** *Steady-state responses of the pressures to input current*

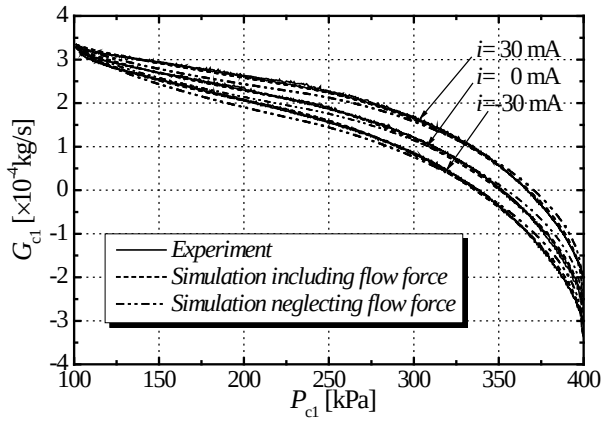


**Fig. 9:** *Flow rate vs. pressure at input current of –30 mA, 0 mA and 30 mA*

The results of the simulation including flow force and experiment are in a good agreement. Due to the influence of flow force, the distance between the nozzle and flapper increases with load pressure. The comparison between the results of the simulation neglecting the flow force and that of the experiment shows this distance to be below the equilibrium distance when the load pressure was below the equilibrium pressure. Conversely, this distance was above the equilibrium distance when the load pressure was above the equilibrium pressure.

The dynamic response of the servo valve is expressed using the step response and frequency response

of the control pressure with respect to the input current.

Various step input currents were applied to the model and experimental setup with both control ports closed. The input current was varied using step-up signals with magnitudes of ±10%, ±20% and ±30% of the rated current. As shown in Fig. 10, the results of the simulation including flow force and experiment are in a good agreement. However, neglecting the flow force produces a steady state error of about 32% between the simulated and experimental results. This shows that flow force has the effect of reducing the pressure gain of the servo valve.

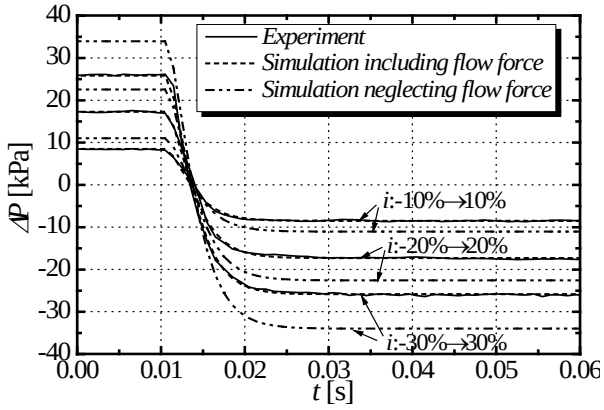


**Fig. 10:** *Step response of the differential pressure to step-up inputs of ±10 %, ±20 % and ±30 % of the rated input current*

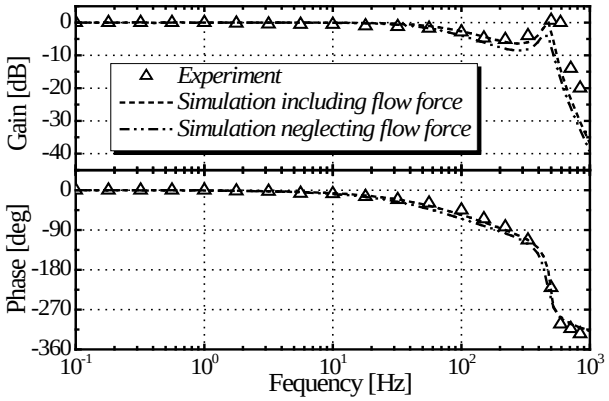


**Fig. 11:** *Frequency response of the differential pressure measured at 0 mA DC input superimposed by ±5 mA sinusoid, magnitude is normalized by static gain*

The frequency response was obtained by superimposing a 5 mA swept sinusoidal current on a biased zero input current and is summarized in the bode diagram shown in Fig. 11. From this bode diagram we can see that the gains for both the experiment and model descended to 3 dB at about 100 Hz. At about 400 Hz a peak appears in the bode diagram and corresponds to the resonant frequency of the armature-flapper. The flow force has the effect of slightly improving the break-point frequency.

# 5 Linear Model

## 5.1 Linear Model Derivation

A linear model is often more useful than non-linear models in servo system designs. Therefore, we will derive a linear model to approximate the non-linear model given in the previous sections. The linear model approximation is made with respect to the state of equilibrium by blocked control flow with zero input current. The control pressures at equilibrium, $P_{c10}$ and $P_{c20}$, can be calculated from Eq. 6, 7 and 8 as Eq. 16, when the flow rate through the fixed orifice equals that through the nozzle-flapper; the flow state at the fixed orifice is subsonic and that at the nozzle-flapper is sonic.

$$C_o P_s \varphi(P_s, P_c) = C_n P_c \varphi(P_c, P_a) \tag{18}$$

Because the two control pressures at equilibrium are not zero, the pressure variations and flow rate variations dynamics to the input current variation derived in Appendix A, have the forms shown in Fig. 12. This block diagram shows that a nozzle-flapper type servo valve can be validly represented by an approximate fourth order model. From the physical parameters of the valve, we easily find that the break-point frequency of the toque-motor is approximately 2230 rad/s, the natural frequency of the armature-flapper is 2953 rad/s, the damping ratio is 0.012 and the break-point frequency of the air dynamics in the control chamber is 565 rad/s. The air dynamics in the control chamber are more significant for the low frequency dynamic response of the valve, in spite of the very small volume (0.7 $cm^3$) of the control chamber. Compared to a pneumatic control system consisting of actuators with a slow response (~20Hz), a nozzle-flapper type servo valve has a relatively quick response.

In the servo valve model, if the control ports are connected to actual loads (such as an air cylinder), the control side volumes, $V_1$ and $V_2$, can be considered approximately equal to the load chamber volume because of relatively small volume of the servo valve control chambers. If we neglect the dynamic response of the toque-motor and armature-flapper, then the servo valve outputs, consisting of pressure variations, $\Delta P_{c1}$, and $\Delta P_{c2}$, and flow rate variations, $\Delta G_{c1}$, and $\Delta G_{c2}$, have the simplified forms:

$$\dot{\boldsymbol{X}} = \mathbf{A}\boldsymbol{X} + \boldsymbol{B}\Delta\boldsymbol{i} \tag{19}$$

$$\boldsymbol{y} = \mathbf{D}\boldsymbol{X} + \boldsymbol{E}\Delta\boldsymbol{i} \tag{20}$$

where, $\boldsymbol{X}$, and $\boldsymbol{y}$ are the state vector and output vector respectively and $\mathbf{A}$, $\boldsymbol{B}$, $\mathbf{D}$ and $\boldsymbol{E}$ are obtained in Appendix A.

$$\boldsymbol{X} = \begin{bmatrix} \Delta P_{c1} & \Delta P_{c2} \end{bmatrix}^T$$

$$\boldsymbol{y} = \begin{bmatrix} \Delta \boldsymbol{P}_{c1} & \Delta \boldsymbol{G}_{c1} & \Delta \boldsymbol{P}_{c2} & \Delta \boldsymbol{G}_{c2} \end{bmatrix}^T$$

$$\mathbf{A} = \begin{bmatrix} \dfrac{a_{o1} - a_{n11}}{K_{c1}} & \dfrac{a_{n21}}{K_{c1}} \\ \dfrac{a_{n12}}{K_{c2}} & \dfrac{a_{o2} - a_{n22}}{K_{c2}} \end{bmatrix}, \quad \boldsymbol{B} = \begin{bmatrix} \boldsymbol{a}_{ni1} \\ \boldsymbol{a}_{ni2} \end{bmatrix}$$

$$\mathbf{D} = \begin{bmatrix} 1 & 0 \\ a_{o1} - a_{n11} & a_{n21} \\ 0 & 1 \\ a_{n12} & a_{o2} - a_{n22} \end{bmatrix}, \quad \boldsymbol{E} = \begin{bmatrix} 0 \\ \boldsymbol{a}_{ni1} \\ 0 \\ \boldsymbol{a}_{ni2} \end{bmatrix}$$

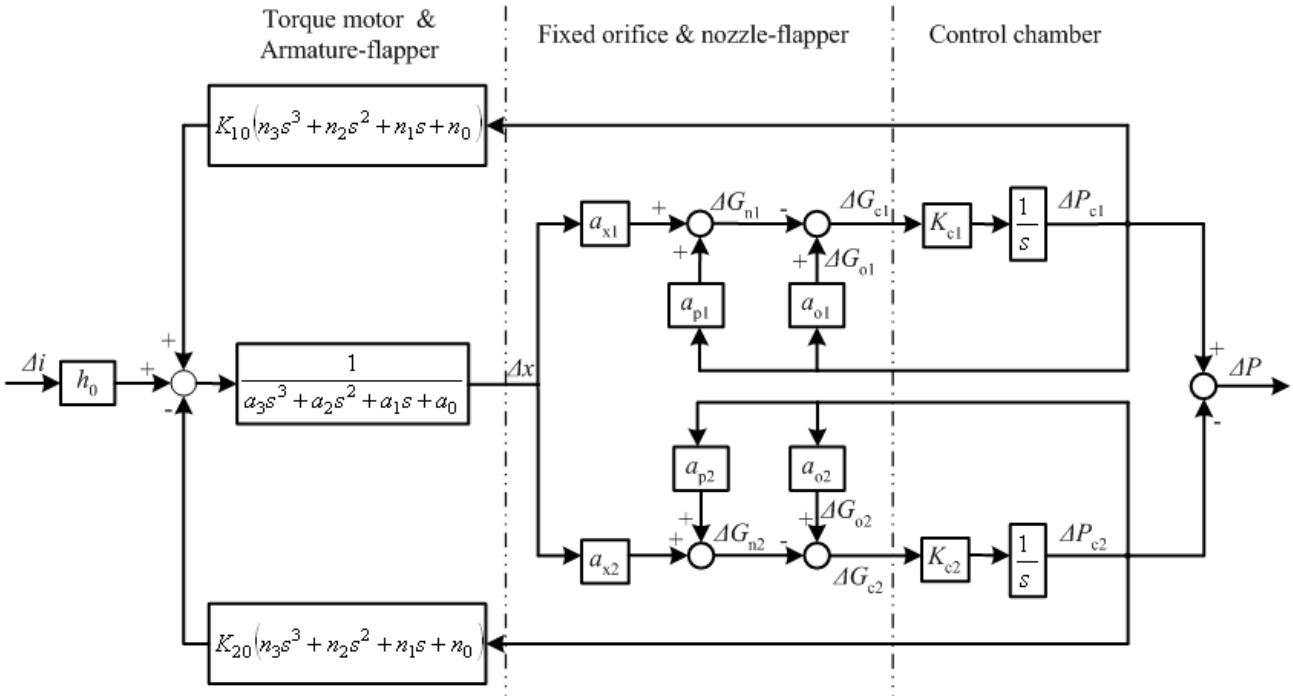


**Fig. 12:** *Schematic of a linear model of a 4-port pneumatic nozzle-flapper type servo valve including the control chambers*

### 5.2 Linear Model Verification

To verify that the linear model in Fig. 12 and the order-reduced linear model in Eq. 19 and 20 exactly capture the fundamental dynamics of the servo valve, the responses to the various step input currents were simulated using these models and the complete nonlinear model. These were performed both with and without the load chambers. In view of the input range of ±30 % for the actual control system, the amplitude of the change in input current was set to $i$=±10, ±20 and ±30 mA. If two identical load chambers ($V_1$=$V_2$=95 cm$^3$) are connected to the control ports of the servo valve, the air dynamics in the load chamber will be as stated in Eq. 16.

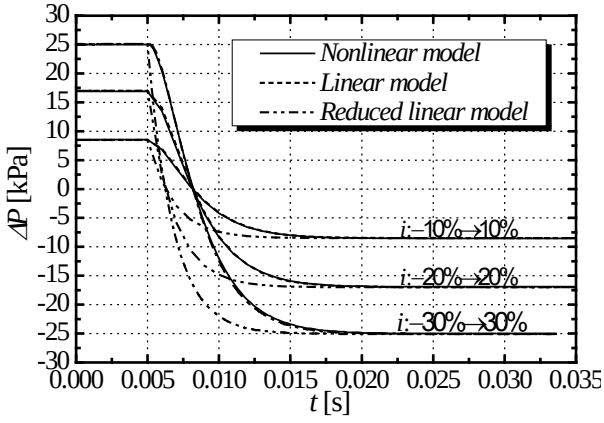


**Fig. 13:** *Step response of the differential pressure for the servo valve without load chambers. Input steps are ±10 %, ±20 % and ±30 % of the rated input current*

Figure 13 shows the simulated results for the response of the differential pressure of the three models without load chambers. When the control chamber is extremely small, the linear model has very good agreement with the complete nonlinear model. Figure 13 also clearly demonstrates a close correlation between the standard linear model in Fig. 12 and the complete nonlinear model for changes in input current of up to ±30 mA. The dynamic response of the order-reduced model is faster than both the standard linear and the complete nonlinear models because the dynamic lag of the torque motor the armature-flapper is neglected.

Figure 14 shows the simulated results for the response of the differential pressure of the three models with 95 cm$^3$ load chambers connected. Again, this shows good agreement between the results of the three models and that of the experiment. This shows that the dynamics of a servo valve within a servo system can be adequately captured by the order-reduced model specified in Eq. 19 and 20.

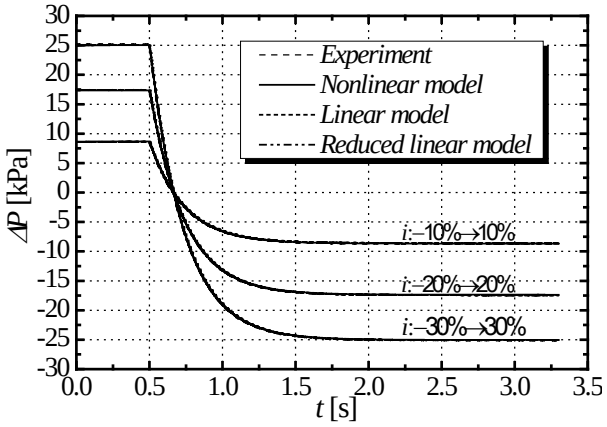


**Fig. 14:** *Step response of the differential pressure for the servo valve including 95 cm³ load chambers Input steps are ±10 %, ±20 % and ±30 % of the rated input current*

We examine the adaptive range of the order-reduced model in the control system by varying the volume of the load chambers. Figure 15 shows the error of 64% rising time, $e_{rt}=(t_1-t_n)/t_n$, between the order-reduced model and the complete nonlinear model when the step input is ±20 mA at the different load volumes. This rising time error is less than 3% when the volume is more than 38 cm$^3$. At this volume, the break-point frequency of the control chamber is 10.85 rad/s. Comparing this with a 2230 rad/s break-point frequency and 2953 rad/s natural frequency for the torque-motor and armature-flapper respectively, it can clearly be seen that the dynamics inside the control chamber dominate the servo valve dynamics when the volume of the controlled load chambers is sufficiently large.

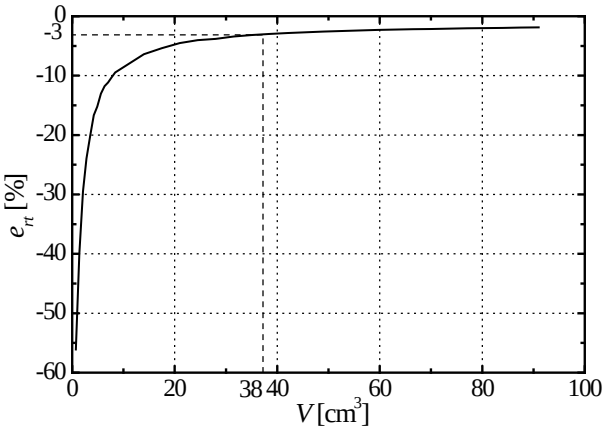


**Fig.15:** *Error of 64% rising time between the order-reduced model and the complete nonlinear model at a ±20 mA step input (the error becomes -3% at the volume of 38 cm³)*

## 6 Conclusions

In this paper, a complete nonlinear model of a 4-port pneumatic nozzle-flapper type servo valve is proposed which includes the influence of the flow force on the flapper. A practical method for determination of the flow force using an experimental approach is also proposed. Static and dynamic responses of both the simulated and experimental results show good agreement. By comparing the complete model and that neglecting the flow force, the influence of the flow force was clearly demonstrated. A linear model, which was derived from the complete nonlinear model, showed an applicable range of about 30% of the rated input current. A general order-reduced linear model is proposed and it is suitable for systems with large load volumes.

## Nomenclature

| | | |
|---|---|---|
| $A_1$ | nozzle area (see Fig.3) | [m$^2$] |
| $A_2$ | nozzle exit area (see Fig.3) | [m$^2$] |
| $B_f$ | damping coefficient of armature-flapper | [Nms] |
| $b_{o1}$, $b_{o2}$ | critical pressure ratio of left and right fixed orifice | [--] |
| $b_{n1}$, $b_{n2}$ | critical pressure ratio of left and right nozzle-flapper | [--] |
| $C_{o1}$, $C_{o2}$ | sonic conductance of left and right fixed orifice | [m$^4$s/kg] |
| $C_{n1}$, $C_{n2}$ | sonic conductance of left and right nozzle-flapper | [m$^4$s/kg] |
| $C_{n10}$, $C_{n20}$ | sonic conductance of left and right nozzle-flapper at zero input current | [m$^4$s/kg] |
| $d_1$ | nozzle diameter (see Fig.3) | [m] |
| $d_2$ | nozzle exit diameter (see Fig.3) | [m] |
| $e_{rt}$ | 64% rising time error | [%] |
| $F_1$, $F_2$ | flow force on left and right side of flapper | [N] |
| $G_{c1}$, $G_{c2}$ | mass flow rate of left and right control side | [kg/s] |
| $G_{o1}$, $G_{o2}$ | mass flow rate through left and right fixed orifice | [kg/s] |
| $G_{n1}$, $G_{n2}$ | mass flow rate through left and nozzle-flapper | [kg/s] |
| $i$ | input current | [mA] |
| $J$ | armature-flapper moment of interia with the respect to its mass centre | [kg·m$^2$] |
| $K_a$ | rotational stiffness of flex-tube | [Nm/rad] |
| $K_F$ | spring constant of flapper rod bending | [N/m] |
| $K_{f1}$, $K_{f2}$ | flow force coefficient of left and right side of flapper | [N/Pa] |
| $K_m$ | electromagnetic rotational stiffness | [Nm/rad] |
| $K_n$ | Flow rate coefficient of nozzle-flapper | [--] |
| $K_i$ | torque-motor gain | [Nm/mA] |
| $K_T$ | spring constant of flex-tube bending | [N/m] |
| $l_a$ | distance from nozzle to centre of rotation (see Fig.2) | [m] |
| $l_t$ | flex-tube length (see Fig.2) | [m] |
| $l_f$ | flapper length (see Fig.2) | [m] |
| $m_{o1}$, $m_{o2}$ | subsonic index of left and right | [--] |

| | | |
|---|---|---|
| | fixed orifice | |
| $m_{n1}$, $m_{n2}$ | subsonic index of left and right nozzle-flapper | [--] |
| $P_a$ | atmosphere pressure | [Pa] |
| $P_{c1}$, $P_{c2}$ | left and right side control pressure | [Pa] |
| $P_d$ | pressure at downstream of restriction | [Pa] |
| $P_s$ | supply pressure | [Pa] |
| $P_u$ | pressure at upstream of restriction | [Pa] |
| $R$ | gas constant | [$m^2/s^2K$] |
| $V_1$, $V_2$ | volume of left and right control chamber | [$m^3$] |
| $T_e$ | time constant due to eddy currents | [s] |
| $T_f$ | torque caused by flow force on flapper | [Nm] |
| $t_l$ | 64% rising time of order-reduced linear model | [s] |
| $t_n$ | 64% rising time of complete nonliner model | [s] |
| $T_s$ | torque caused by deformation of flex-tube | [Nm] |
| $T_t$ | torque caused by electromagnetic forces | [Nm] |
| $x$ | flapper tip displacement | [m] |
| $x_f$ | distance from flapper tip to each nozzle at zero input current | [m] |
| $\Delta P$ | differential pressure between both control sides $\Delta P=P_{c1}-P_{c2}$ | [Pa] |
| $\alpha$ | armature-flapper deflection | [rad] |
| $\theta$ | air temperauture | [K] |
| $\kappa$ | ratio of specfic heat $\kappa$=1.4 | [--] |
| $\rho$ | air density for standard conditions | [$kg/m^3$] |

## References


**Araki, K**. 1965. Nozzle-Flapper Static Characteristics in Pneumatic Servomechanisms, *Transactions of SICE of Japan*, 1-2 pp. 182–188. (in Japanese)

**Crnojevic, C., Roy. G., Bettahar, A. and Florent, P.** 1997. The Influence of the Regulator Diameter and Injection Nozzle Geometry on the Flow Structure in Pneumatic Dimensional Control Systems, *Trans. ASME J. of Fluids Engineering*, Sep. pp. 609-615.

**Grodić, D., Babić. M. and Jovičić, N.** 2004. Modelling of Spool Position Feedback Servovalves, *International Journal of Fluid Power*, Vol. 5, No. 1, pp. 37-50.

**Kagawa, T.** 1985. Heat Transfer Effects on the Frequency Response of a Pneumatic Nozzle Flapper, *ASME-DSMC*, Dec. pp. 332-336.

**Kim, D. H. and Tsao, T. C.** 2000 A Lineariezd Electrohydraulic Servovalve model for Valve Dynamics sensitivity Analysis and Control System Design. *ASME-DSMC*, Vol.122, pp. 179-187

**Lin, S. L. and Akers, A.** 1991. Dynamic Analysis of a Flapper Nozzle Valve. *ASME-DSMC*, Vol. 111, pp. 163-167

**Merritt, H. E.** 1967. *Hydraulic Control Systems*, Wiley, New York.

**Ohuchi, H. and Ikebe. Y.** 1980 Self-Excited Oscillation of Nozzle-Flapper Valves, *Hydraulic and pneumatic*, Vol.11, No. 4, pp. 239-245. (in Japanese)

**Oneyama, N., Takahashi, T. Terashima, Y., Kuroshita, K. and Kagawa, T.** 2003. Study and suggestion on Flow-rate Characteristics of Pneumatic Components, *Proceeding of the Seventh Triennial International Symposium on Fluid Control, Measurement and Visualization*, Sorrento, Italy, Aug.

**Shearer, J. E.** 1956. Study of Pneumatic Process in the Continuous Control of Motion with Compressed Air-I, II, *Trans. ASME*, Feb. pp. 233-249.

**Thayer, W. J.** 1958, Rev. 1965. Transfer functions for Moog servovalves, *Moog Technical Bulletion* 103

**Toyokura, T. and Kamemoto, K.** 1976 *Fluid dynamic*, Jitsukyou Press, pp.61-63. (in Japanese)

**Urata, E.** 1999. Dynamics of elastic structures in servovalve toque motor, *Bath Workshop on Power Transmission and Motion Control*, (PTMC99). pp. 183-186.

**Urata, E.** 2004. Influence of eddy current on torque-motor dynamics, *4th IFK Workshop*, Mar 24. pp. 71-82.

**Urata, E.** 2004. One-degree-of-freedom Model for Torque-motor Dynamics, *International Journal of Fluid Power*, Vol. 5, No. 2, pp. 35-42.

**Urata, E. and Yamashina, C.** 1998. Influence of Flow Force on the Flapper of a Water Hydraulic Servovalve, *JSME International Journal*, Series B, Vol. 41, No. 2, pp. 278-285

**Urata, E., Miyakawa, S., Yamashina, C., Nakao, Y., Usami, Y. and Shinoda, M.** 1998. Development of Water Hydraulic Servovalve, *JSME International Journal*, Series B, Vol. 41, No. 2, pp. 286-294

**Wakui, S.** 2003. Incline compensation control using an air-spring type active isolated apparatus, *Precision Engineering*, 27(2). pp. 170-174

**Zalmanzon, L. A.** 1965. *Components for Pneumatic Control Instruments*, Pergamon Press.

**Zhang, Y., Kagawa, T., Yamamoto, T. and Nakata, T.** 2003. Influence of Flow Jet on Nozzle Flapper Systems, *Transactions of the Japan fluid power system society*, Vol. 34, No. 3. pp 55-61. (in Japanese)

**Tao Wang**
Born on December 1971. Received his M. Sc from the Beijing Institute of Technology (China) in 1999. Now he is a graduate student of at the Department of Mechano-Micro Engineering at the Tokyo Institute of Technology for doctoral degree, in Japan. His primary research fields are modeling and control of pneumatic servo system and pneumatic components characteristics measurement.

**Maolin Cai**
Born on January 1972. Received his M. Sc degree from the Beijing Institute of Technology (China) in 1996 and Ph. D from the Tokyo Institute of Technology (Japan) in 2002. He has being working at the Precision and Intelligence Laboratory of this institute. His primary research interests are saving energy of pneumatic system, fluid measurement and control.

**Kenji Kawashima**
Born on July 1968. Received his Ph. D degree from the Tokyo Institute of Technology (Japan) in 1997. He was working as an associate professor at the Precision and Intelligence Laboratory of this institute. His primary research interests are fluid measurement and control, robot engineering.

**Toshiharu Kagawa**
Born on November 1950. Received his M. Sc and Ph. D degree from the Tokyo Institute of Technology in Japan. He was working as a professor at the Precision and Intelligence Laboratory of this institute. His primary research interests are fluid measurement and control.

## Appendix A: Derivation of the linear model

From the armature-flapper model in Eqs. 4 and 5, a s-function, relating the displacement due to input current and the control pressure can be derived as follows:

$$\frac{\Delta x(s)}{h_0 \Delta i(s) + \left(n_3 s^3 + n_2 s^2 + n_1 s + n_0\right)\left(K_{10}\Delta P_{c1}(s) - K_{20}\Delta P_{c2}(s)\right)} = \frac{1}{a_3 s^3 + a_2 s^2 + a_1 s + a_0} \quad \text{(A1)}$$

where

$$a_0 = K_a - K_m$$

$$a_1 = B_f + K_a T_e$$

$$a_2 = n_2 = J + B_f T_e$$

$$a_3 = n_3 = J T_e$$

$$h_0 = K_i l_a / \left(1/K_F + 1/K_T\right)$$

$$n_0 = l_a^2 / \left(1/K_F + 1/K_T\right) + K_a - K_m$$

$$n_1 = T_e l_a^2 / \left(1/K_F + 1/K_T\right) + B_f + K_a T_e$$

$K_{10}$ is $K_{f1}$ at the equilibrium position.
$K_{20}$ is $K_{f2}$ at the equilibrium position.

By linearizing Eq. 6 at the equilibrium position, the flow rate variation at the fixed orifice can be obtained from the control pressure variation as follows:

$$\Delta G_{o1} = a_{o1}\Delta P_{c1} \quad \text{(A2)}$$

$$\Delta G_{o2} = a_{o2}\Delta P_{c2} \quad \text{(A3)}$$

where

$$a_{o1} = \left.\frac{dG_{o1}}{dP_{c1}}\right|_{P_{c1}=P_{c10}}, \quad a_{o2} = \left.\frac{dG_{o2}}{dP_{c2}}\right|_{P_{c2}=P_{c20}}$$

By linearizing Eq. 6 and 8 at the equilibrium position, the flow rate variation at the nozzle-flapper can be obtained from the displacement variation and the control pressure variation as follows:

$$\Delta G_{n1} = a_{x1}\Delta x + a_{p1}\Delta P_{c1} \quad \text{(A4)}$$

$$\Delta G_{n2} = a_{x2}\Delta x + a_{p2}\Delta P_{c2} \quad \text{(A5)}$$

where

$$a_{x1} = \left.\frac{\partial G_{n1}}{\partial x}\right|_{\substack{x=0 \\ P_{c1}=P_{c10}}}, \quad a_{p1} = \left.\frac{\partial G_{n1}}{\partial P_{c1}}\right|_{\substack{x=0 \\ P_{c1}=P_{c10}}}$$

$$a_{x2} = \left.\frac{\partial G_{n2}}{\partial x}\right|_{\substack{x=0 \\ P_{c2}=P_{c20}}}, \quad a_{p2} = \left.\frac{\partial G_{n2}}{\partial P_{c2}}\right|_{\substack{x=0 \\ P_{c2}=P_{c20}}}$$

In the order-reduced model, neglecting the dynamics of the torque motor and armature-flapper, the flow rate variations at the nozzle-flappers are linearized at the equilibrium position from the input current variation and both of the control pressure variations as follows:

$$\Delta G_{n1} = a_{n11}\Delta P_{c1} + a_{ni1}\Delta i + a_{n12}\Delta P_{c2} \quad \text{(A6)}$$

$$\Delta G_{n2} = a_{n21}\Delta P_{c1} + a_{ni2}\Delta i + a_{n22}\Delta P_{c2} \quad \text{(A7)}$$

where

$$a_{n11} = \left.\frac{\partial G_{n1}}{\partial P_{c1}}\right|_{\substack{i=0 \\ P_{c1}=P_{c10} \\ P_{c2}=P_{c20}}}, \quad a_{ni1} = \left.\frac{\partial G_{n1}}{\partial i}\right|_{\substack{i=0 \\ P_{c1}=P_{c10} \\ P_{c2}=P_{c20}}},$$

$$a_{n12} = \left.\frac{\partial G_{n1}}{\partial P_{c2}}\right|_{\substack{i=i_0 \\ P_{c1}=P_{c10} \\ P_{c2}=P_{c20}}}$$

$$a_{n21} = \left.\frac{\partial G_{n2}}{\partial P_{c2}}\right|_{\substack{i=0 \\ P_{c1}=P_{c10} \\ P_{c2}=P_{c20}}}, \quad a_{ni2} = \left.\frac{\partial G_{n2}}{\partial i}\right|_{\substack{i=0 \\ P_{c1}=P_{c10} \\ P_{c2}=P_{c20}}},$$

$$a_{n22} = \left.\frac{\partial G_{n2}}{\partial P_{c2}}\right|_{\substack{i=0 \\ P_{c1}=P_{c10} \\ P_{c2}=P_{c20}}}$$